

Properties of Amine-Containing Ligands That Are Necessary for Visible-Light-Promoted Catalysis with Divalent Europium

Ramiro Barraza, Jr., Alexander G. Sertage, Aravind B. Kajjam, Cassandra L. Ward, Jacob C. Lutter, H. Bernhard Schlegel, and Matthew J. Allen*



Cite This: *Inorg. Chem.* 2022, 61, 19649–19657



Read Online

ACCESS |



Metrics & More

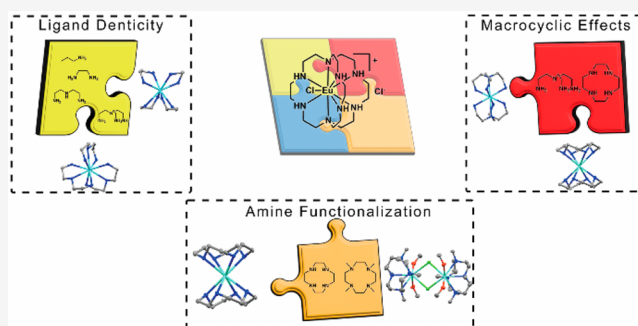


Article Recommendations



Supporting Information

ABSTRACT: We describe a study of the influence of amine-containing ligands on the photoredox-relevant properties of Eu^{II} toward the rational design of Eu^{II} -containing catalysts for visible-light-promoted photoredox reactions. We report our observations of the effects of the degree of functionalization of amines, denticity, and macrocyclic ligands on the absorbance of Eu^{II} . Ligands that contain secondary amines bathochromically shift the absorbance of EuCl_2 relative to ligands that contain primary or tertiary amines. Similarly, ligands of larger denticity have a larger bathochromic shift of the absorbance than ligands of smaller denticity. We observed that macrocyclic ligands have a larger effect on the absorbance of EuCl_2 than nonmacrocyclic ligands. Also, we report the photoredox reactivity of four new Eu^{II} -containing complexes. These observations are potentially influential in understanding the ligand properties that promote the use of Eu^{II} in visible-light-promoted photoredox catalysis.



INTRODUCTION

The ability to efficiently replace or install functional groups in synthetically valuable compounds is desired by synthetic chemists. Light-activated precatalysts can initiate these critical reactions by converting light energy into synthetically useful chemical energy.^{1–3} Visible-light-promoted photoredox catalysis uses low-energy visible light to promote reactions that would otherwise be difficult to achieve or require harsh reaction conditions, such as heat or UV light, using organic dyes or metal complexes.^{4–6} Various metals including d- and f-block metals, such as Ru, Ir, Cu, Ce, Sm, and Eu, catalyze organic reactions via metal-assisted photoredox catalysis.^{7–21} Recently, the first visible-light-promoted photoredox catalyst based on Eu was reported, $\text{Eu}^{\text{II}}\text{ICl}_2$ (Figure 1).²² The complex has an excited-state electrochemical potential of -3.2 V versus normal hydrogen electrode (NHE). This potential is one of the most negatively reported excited-state potentials for metal-

based photoredox catalysis and is more negative than the common reducing agent SmI_2 in the presence of hexamethylphosphoramide.^{23,24} The essential properties of **1** that are required for visible-light-promoted photocatalysis with Eu^{II} are unclear, and to design new ligands that promote photoredox catalysis with Eu^{II} , the effects of the ligand properties must be elucidated. Because the reported catalyst based on Eu^{II} involved octaaza ligand **1**, we hypothesized that studying the influence of a set of amine-containing ligands on the electrochemical and photophysical properties of Eu^{II} would reveal the ligand attributes necessary to promote reactivity in visible-light-promoted reductions.

Azacryptand **1** causes a shift in the absorbance of the resulting Eu^{II} -containing complex to visible light relative to complexes of ethereal cryptand **2**.^{22,25} On the basis of the absorbance of these two ligands and other complexes of Eu^{II} ,^{26–28} donor atoms softer than O are important to the ability of Eu^{II} to absorb visible light. A recent report described that complexes of Eu^{II} that have more amine donor atoms led to greater bathochromic shifts in absorbance, longer lifetimes, and more negative peak anodic potentials.²⁹ However, via a

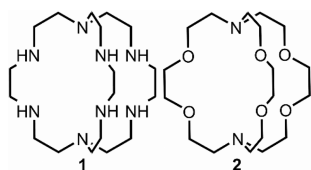
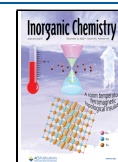


Figure 1. Ligands that bind Eu^{II} resulting in complexes with different spectroscopic properties: $\text{Eu}^{\text{II}}\text{ICl}_2$ absorbs visible light, and $\text{Eu}^{\text{II}}\text{2Cl}_2$ absorbs UV light.

Received: August 13, 2022

Published: November 23, 2022



comparison of ligands **1** and **2** with respect to the absorption of visible light and reactivity when complexed to Eu^{II} , it is unclear how many amines are needed, if primary, secondary, and tertiary amines are equivalent in shifting the properties of Eu^{II} , if macrocyclic structures are important, and what denticity reagents promote visible-light absorption and subsequent reactivity. Here, we report our findings focused toward understanding the ligand properties that provide favorable environments for visible-light-promoted photoredox catalysis using Eu^{II} .

RESULTS AND DISCUSSION

To evaluate the influence of the degree of amine functionalization, the macrocyclic effect, and denticity on the spectroscopic properties and reactivity of Eu^{II} , we studied mixtures of EuCl_2 with the ligands in Figure 2. Ligands **3–19** include

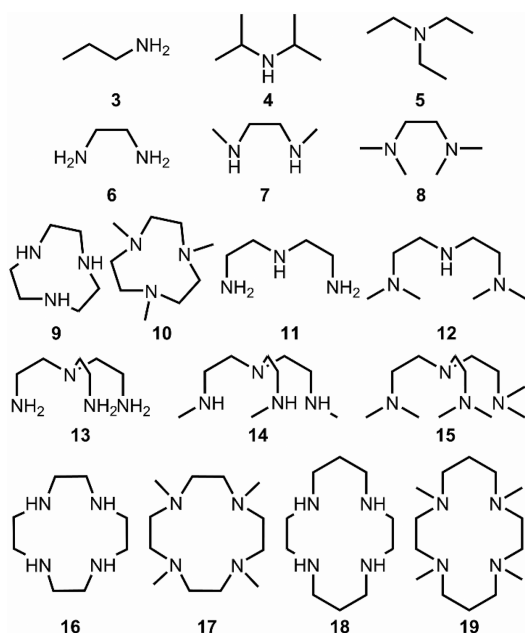


Figure 2. Amine-containing ligands used in this study.

monodentate, bidentate, tridentate, tetradentate, linear, branched, and macrocyclic ligands with varying degrees of functionalization. All ligands were purchased or synthesized following reported procedures.^{30,31} Once mixtures of each ligand with EuCl_2 were prepared, and the absorbance, excitation, and emission of each mixture were measured to evaluate the effect of each ligand on the spectroscopic properties of EuCl_2 .

An initial screening procedure was performed to select only ligands that resulted in the absorption of visible light. Each ligand, **3–19**, was mixed with EuCl_2 in methanol (MeOH), and the absorbance and luminescence of the resulting solutions were studied. MeOH was used as the solvent because ligands **3–19** and EuCl_2 are soluble in MeOH and because MeOH was used in reported visible-light-promoted photoredox reactions with Eu^{II} .²² All solutions were prepared in a dry glovebox because Eu^{II} readily oxidizes to Eu^{III} when exposed to air. Solutions of each ligand (31.1–38.2 mM, 10 equiv) in MeOH were stirred with methanolic solutions of EuCl_2 (3.11–3.82 mM, 1 equiv) to form Eu^{II} –ligand mixtures. Each solution was prepared in a 10:1 ligand-to-metal ratio in an attempt to

saturate the coordination sites of Eu^{II} because Eu^{II} typically has a coordination number of eight or nine. To confirm that monodentate ligands saturated the coordination sphere of Eu^{II} , we also prepared those ligands at 20:1 and 50:1 ligand-to-metal ratios, and no spectroscopic differences in the absorbance peaks were observed, indicating that saturation was achieved at a 10:1 ligand-to-metal ratio. Absorbance spectra were acquired for each Eu^{II} –ligand mixture (Figures S1–S17). The absorption spectra of each amine-containing ligand mixed with EuCl_2 was assessed for absorbance in the visible-light range, 380–700 nm. EuCl_2 has an absorption maximum at 330 nm that trails into the visible-light region to 430 nm. Although the absorption of EuCl_2 trails into the visible-light region, this tail does not extend far enough to enable efficient absorption of visible light to promote visible-light-promoted photochemical reactions.²² On the basis of these observations, mixtures that have absorption peaks within or trailing further into the visible-light range are potentially viable as visible-light-promoted photoredox catalysts. Of ligands **3–19**, those that led to shifts fitting these criteria were 1,4,7-triazacyclononane (TACN, **9**), *N,N,N*-trimethyl-1,4,7-triazacyclononane (Me_3TACN , **10**), tris(2-aminoethyl)amine (TREN, **13**), 1,4,7,10-tetraazacyclododecane (cyclen, **16**), and *N,N,N,N*-tetramethyltetraazacyclododecane (Me_4Cyclen , **17**).

Degree of Amine Functionalization. To evaluate the influence of the degree of amine functionalization on EuCl_2 , we compared the spectroscopic properties of ligands **3–19**. We compared pairings of primary, secondary, or tertiary amine-containing ligands to elucidate how each degree of functionalization influences the spectroscopic properties of EuCl_2 . Of the pairings of ligands **3–19**, the absorption spectra of ligands **3–8**, **11**, **12**, **18**, and **19** did not differ from each other; therefore, we cannot elucidate trends regarding the effect of the degree of functionalization of the amine for these ligands. However, the absorption spectra of ligands **9**, **10**, **13**, **16**, and **17** (Figure 3) contain notable shifts. **9** and **10** are both

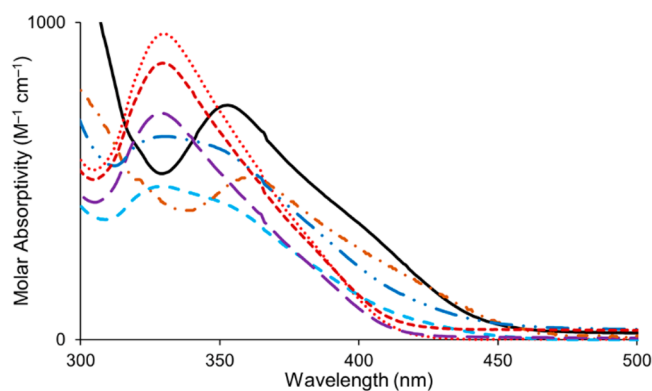


Figure 3. UV–visible spectra of complexes of Eu^{II} –ligand (1.27–1.56 mM) in MeOH that show the effect of the degree of amine functionalization on absorbance: Eu^{II} TACN (**9**, —), Eu^{II} Me_3TACN (**10**, ···), Eu^{II} TREN (**13**, ---), Eu^{II} Me_3TREN (**14**, — · —), Eu^{II} cyclen (**16**, - - -), Eu^{II} Me_4Cyclen (**17**, — · — · —), and EuCl_2 (— · — · —).

tridentate, macrocyclic amine-containing ligands. Ligand **9** contains three secondary amines, and ligand **10** contains three tertiary amines. In the presence of EuCl_2 , **9** has an absorption maximum that is more bathochromically shifted at 353 nm than its tertiary derivate, **10**, which has an absorption maximum at 330 nm. The absorption maximum of **9**, in the

presence of EuCl_2 , trails to approximately 470 nm, and the absorption maximum of **10** trails to 430 nm. **13** and N,N,N',N'' -trimethyl[tris(2-aminoethyl)amine] (Me_3TREN , **14**) are tetradentate, branched amine-containing ligands. Ligand **13** contains three primary amines and one tertiary amine, and ligand **14** contains three secondary amines and one tertiary amine. A mixture of EuCl_2 and **13** has an absorption maximum at 330 nm and a prominent shoulder around 350–360 nm. The shoulder of the mixture of EuCl_2 and **13** trails to 450 nm. The absorption spectra of **14**, in the presence of EuCl_2 , parallels the spectra of a mixture of EuCl_2 and **10**, which has an absorption maximum at 330 nm and trails to 420 nm. **16** and **17** are tetradentate, macrocyclic ligands. Ligand **16** contains four secondary amines, and ligand **17** contains four tertiary amines. A mixture of **16** and EuCl_2 has an absorption maximum at 362 nm that trails to 470 nm. **17**, in the presence of EuCl_2 , has an absorption maximum at 340 nm with a shoulder at 350 nm that trails to 470 nm.

Comparing ligands **9**, **10**, and **13**–**17**, we observed that ligands that contain secondary amines have a larger effect on the absorption of EuCl_2 than ligands that contain mostly tertiary amines. For example, ligands **9** and **13** shift the absorption spectra of EuCl_2 and trail past 450 nm, but their tertiary amine derivatives, **10** and **14**, do not have an effect on the absorption spectra of EuCl_2 . **16** and **17** both bathochromically shift the absorption of EuCl_2 and trail to 470 nm; however, **16** has a larger bathochromic shift than **17**. These observations suggest that ligands that contain secondary amines have a larger bathochromic effect than primary or tertiary amines on the absorption of EuCl_2 . This ability to shift absorbance is a favorable characteristic for the design of visible-light-promoted photocatalysts.

Macrocycles. On the basis of the spectroscopic observations of ligands **3**–**19** with Eu^{II} , ligands with strong chelating effects, such as macrocycles, differ from ligands with weaker chelating effects, such as branched or linear ligands. To understand how macrocyclic ligands compared to similar nonmacrocyclic ligands with respect to the ability to influence the properties of Eu^{II} , ligands **10**, N,N,N',N' -tetramethyldiethylenetriamine (Me_4DETA , **12**), N,N,N',N',N'',N'' -hexamethyl[tris(2-aminoethyl)amine] (Me_6TREN , **15**), and **17** were compared to each other to evaluate the effect of macrocyclic amine-containing ligands on the absorption of EuCl_2 (Figure 4). Ligand **10** is a tridentate macrocyclic ligand that contains three tertiary amines, and ligand **12** is a linear tridentate ligand that contains two tertiary amines and one primary amine. Ligands **10** and **12** did not influence the absorption of EuCl_2 , and mixtures of each ligand with EuCl_2 had absorption maxima at 330 nm that trailed to 420 nm. **15** is a tetradentate, branched ligand that contains four tertiary amines, and **17** is a tetradentate, macrocyclic ligand that contains four tertiary amines. Ligand **15** showed no effect on the absorption of EuCl_2 , with mixtures of **15** and EuCl_2 showing an absorption maximum at 330 nm that trails to 420 nm. Ligand **17** in the presence of EuCl_2 showed an absorption maximum at 340 nm with a shoulder at 350 nm. The absorption maximum of EuCl_2 in the presence of **17** trailed to 470 nm. On the basis of observations using **10**, **12**, **15**, and **17**, macrocycles tend to impart greater shifts in the absorbance wavelengths than otherwise structurally similar nonmacrocyclic counterparts. We observed no shift in the absorbance of EuCl_2 in the presence of 1,4,8,11-tetraazacyclotetradecane (cyclam, **18**). This observation is likely due to

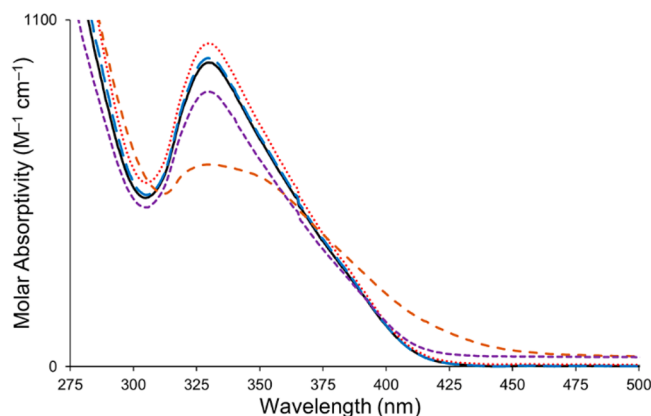


Figure 4. UV–visible spectra of complexes of Eu^{II} –ligand (1.27–1.56 mM) in MeOH that show the effect of macrocycles on absorbance: $\text{Eu}^{\text{II}}\text{Me}_3\text{TACN}$ (**10**, —), $\text{Eu}^{\text{II}}\text{Me}_4\text{DETA}$ (**12**, ···), $\text{Eu}^{\text{II}}\text{Me}_6\text{TREN}$ (**15**, ---), $\text{Eu}^{\text{II}}\text{Me}_4\text{Cyclen}$ (**17**, — —), and EuCl_2 (— —).

steric interactions caused by the propylene groups on cyclam (**18**) inhibiting coordination. The lack of an effect of **10** on the absorbance of EuCl_2 also suggests that ligand denticity has an effect on how much amine-containing ligands influence the absorption of EuCl_2 .

Denticity. To explore how the ligand denticity affects the absorption of EuCl_2 , we compared ligands with similar degrees of functionalization. Specifically, the absorption spectra of the ligands propylamine (**3**), 1,2-diaminoethane (DAE, **6**), **9**, diethylenetriamine (DETA, **11**), **13**, and **16** were compared (Figure 5). Ligands **3**, **6**, **11**, and **13** were clustered for

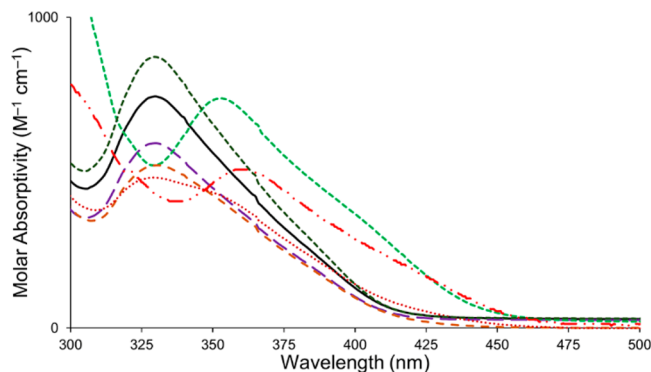


Figure 5. UV–visible spectra of complexes of Eu^{II} –ligand (1.27–1.56 mM) in MeOH that show the effect of denticity on absorbance: Eu^{II} propylamine (**3**, —), $\text{Eu}^{\text{II}}\text{DAE}$ (**6**, — —), $\text{Eu}^{\text{II}}\text{TACN}$ (**9**, light-green ···), $\text{Eu}^{\text{II}}\text{DETA}$ (**11**, dark-green ---), $\text{Eu}^{\text{II}}\text{TREN}$ (**13**, ···), $\text{Eu}^{\text{II}}\text{Cyclen}$ (**16**, — — —), and EuCl_2 (— —).

comparison as nonmacrocyclic ligands, and ligands **9** and **16** were grouped separately because they are macrocycles. **3**, **6**, **11**, and **13** are predominantly primary amine-containing ligands. **9** and **16** are secondary amine-containing macrocyclic ligands. Ligands **3**, **6**, and **11** are monodentate, bidentate, and tridentate, respectively, and the absorbance of each on EuCl_2 had an absorption maximum at 330 nm that trailed to 420 nm, denoting no effect on the absorption of EuCl_2 . **13** is a tetradentate ligand and, in the presence of EuCl_2 , has an absorption maximum at 330 nm with a shoulder around 350–360 nm that trails to 450 nm. **9** is a tridentate secondary amine-containing ligand and has an absorption maximum at 353 nm that trails to 470 nm in the presence of EuCl_2 . **16** is a

tetradentate secondary amine-containing ligand and, in the presence of EuCl_2 , has an absorption maximum at 362 nm that trails to 470 nm. Of the linear and branched ligands **3**, **6**, **11**, and **13**, only **13** influenced the absorption of EuCl_2 . This observation suggests that ligands of larger denticity are necessary to coordinate to EuCl_2 in such a way that the ligand shifts the absorption of Eu^{II} . By comparing macrocyclic ligands **9** and **16**, we observed the same trend. **16** is a tetradentate ligand that shifts the absorption of EuCl_2 by 32 nm compared to a shift of 23 nm from tridentate **9**. In linear, branched, and macrocyclic ligands, ligands of larger denticity tend to produce greater bathochromic shifts of the absorption of EuCl_2 than ligands of smaller denticity. The greater bathochromic shifts might be due to the greater chelating effect associated with larger denticity ligands, suggesting that relatively inert coordination to Eu^{II} might be required to have an impact on the absorption of EuCl_2 .

Crystallography. From the comparisons of functionalization and denticity, we observed that ligands that promote bathochromic shifts in the absorbance of Eu^{II} were either secondary amine-containing macrocycles or ligands with denticities greater than or equal to 3. **9**, **13**, **14**, **16**, and **17** shifted the absorption of EuCl_2 enough to potentially be useful for visible-light-promoted photoredox catalysis. To confirm how **6**, **9**, **11**, **13**, **14**, **16**, and **17** bind to EuCl_2 , X-ray-quality crystals were grown from concentrated solutions of EuCl_2 with **6**, **11**, and **13**. *SHAPE* analyses were performed to assign the geometry of each structure (Tables S1–S8).³²

Some of the crystal structures reported here are for the Eu^{III} -containing complexes. Those structures were grown over many months and oxidized in the process of crystallization. Slow evaporation of a concentrated solution of EuCl_2 and **6** yielded clear, colorless crystals of $[\text{Eu}^{\text{III}}_6\text{Cl}]_3$ (Figure 6a). Two separate batches of these crystals were grown, and both batches of crystals yielded Eu^{III} centers. One batch contained an eight-

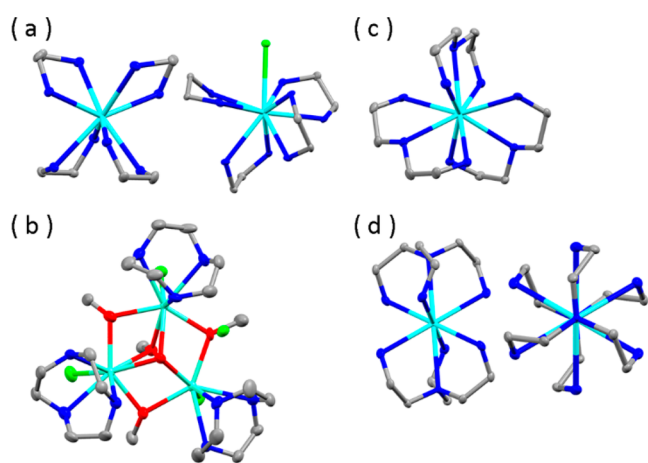


Figure 6. Molecular structures from the crystallographic data of (a) $[\text{Eu}_6\text{Cl}]_3$ (left) and $[\text{Eu}_6\text{Cl}]_6\text{Cl}_2$ (right), (b) $[\text{Eu}^{\text{III}}_3(\text{CH}_3\text{O})_4(\text{OH})_9_3\text{Cl}_3]\text{Cl}$, (c) $[\text{Eu}_{11}_3]\text{Cl}_2$, and (d) $[\text{Eu}_{13}_2]\text{Cl}_2$ (left) perpendicular to and (right) along the C_3 axis. H atoms and noncoordinated counterions are omitted for clarity. Thermal ellipsoids are drawn at 50% probability. Color code: blue, N; gray, C; green, Cl; red, O; seagreen, Eu. The crystallographic data for each structure are available at the Cambridge Crystallographic Data Centre under the following deposition numbers: $[\text{Eu}_6\text{Cl}]_3$, 2121539; $[\text{Eu}^{\text{III}}_3(\text{CH}_3\text{O})_4(\text{OH})_9_3\text{Cl}_3]\text{Cl}$, 2209884; $[\text{Eu}_6\text{Cl}]_6\text{Cl}_2$, 2121631; $[\text{Eu}_{11}_3]\text{Cl}_2$, 2111612; $[\text{Eu}_{13}_2]\text{Cl}_2$, 2111611.

coordinate Eu^{III} -containing complex with three noncoordinating chloride ions (Figure 6a, left). The eight-coordinate complex, $[\text{Eu}^{\text{III}}_6\text{Cl}]_3$, was square-antiprismatic by *SHAPE* (version 2.1) analysis. The second batch contained a nine-coordinate Eu^{III} -containing complex with one coordinating chloride anion, two noncoordinating chloride counterions, and one noncoordinating diaminoethane (Figure 6a, right). *SHAPE* analysis of this complex showed that the nine-coordinate $[\text{Eu}^{\text{III}}_6\text{Cl}]_6\text{Cl}_2$ was similar to the tricapped trigonal-prismatic and muffin geometries. Both crystal structures confirmed that **6** is bidentate. Vapor diffusion at cold temperature of a concentrated solution of EuCl_2 and **9** yielded clear, colorless crystals (Figure 6b). The crystals consisted of a trinuclear complex with three eight-coordinate Eu^{III} centers. The trinuclear complex was found to be $[\text{Eu}^{\text{III}}_3(\text{CH}_3\text{O})_4(\text{OH})_9_3\text{Cl}_3]\text{Cl}$. Each Eu^{III} center is coordinated to one ligand **9**, three methoxide ions, one chloride ion, and one hydroxide ion. Each Eu^{III} center is bridged to another Eu^{III} by methoxide ions, and the hydroxide ion bridges all three Eu^{III} centers. *SHAPE* analysis of each Eu^{III} calculated their geometry to be triangular dodecahedral. These crystals were grown over a long period (multiple months) of time; they likely oxidized slowly during their growth. The $\text{Eu}-\text{N}$ bond lengths for $[\text{Eu}^{\text{III}}_6\text{Cl}]_3$ were 2.48–2.64 Å. The $\text{Eu}-\text{N}$ bond lengths for $[\text{Eu}^{\text{III}}_6\text{Cl}]_6\text{Cl}_2$ were between 2.57 and 2.63 Å, and the $\text{Eu}-\text{Cl}$ bond length was 2.89 Å. The $\text{Eu}-\text{N}$ bond lengths for $[\text{Eu}^{\text{III}}_3(\text{CH}_3\text{O})_4(\text{OH})_9_3\text{Cl}_3]\text{Cl}$ ranged from 2.57 to 2.66 Å. The bond lengths in the aforementioned complexes were in the range of those for the previously reported $\text{Eu}^{\text{III}}-\text{N}$.³³

Slow evaporation of a concentrated solution of EuCl_2 and **11** yielded clear, colorless crystals. The crystals contained a nine-coordinate Eu^{II} with two noncoordinating chloride ions, $[\text{Eu}_{11}_3]\text{Cl}_2$ (Figure 6c). The crystal structure of $[\text{Eu}_{11}_3]\text{Cl}_2$ demonstrates that **11** is tridentate. The nine-coordinate $[\text{Eu}_{11}_3]\text{Cl}_2$ is tricapped trigonal-prismatic by *SHAPE* analysis. Slow evaporation of a slightly yellow, concentrated solution of EuCl_2 and ligand **13** yielded yellow crystals. The yellow crystals were found to contain eight-coordinate Eu^{II} with two noncoordinating chloride ions, $[\text{Eu}_{13}_2]\text{Cl}_2$ (Figure 6d). The crystal structure of $[\text{Eu}_{13}_2]\text{Cl}_2$ demonstrates that ligand **13** is tetradentate when coordinating to Eu^{II} . *SHAPE* analysis for $[\text{Eu}_{13}_2]\text{Cl}_2$ calculated the geometry to be cubic. The $\text{Eu}-\text{N}$ bond lengths for $[\text{Eu}_{11}_3]\text{Cl}_2$ were between 2.73 and 2.84 Å. The $\text{Eu}-\text{N}$ bond lengths for $[\text{Eu}_{13}_2]\text{Cl}_2$ were 2.71–2.79 Å. The $\text{Eu}^{\text{II}}-\text{N}$ bond lengths for $[\text{Eu}_{11}_3]\text{Cl}_2$ and $[\text{Eu}_{13}_2]\text{Cl}_2$ were within the range of previously reported $\text{Eu}^{\text{II}}-\text{N}$ bond lengths.^{22,28,29,34}

Among ligands **3**–**19**, **13**, **16**, and **17** had the largest bathochromic effect on EuCl_2 . To gain insight into how **13** and **16** might be different in their coordination to EuCl_2 compared to their methylated counterparts **14** and **17**, X-ray-quality crystals were grown from concentrated methanolic solutions of **14**, **16**, or **17** and EuCl_2 . Crystals grown from the vapor diffusion of tetrahydrofuran into these concentrated solutions were found to be $\text{Eu}_4\text{14}_4\text{Cl}_8$ and $[\text{Eu}^{\text{II}}_2\text{17}_2(\text{CH}_3\text{OH})_4\text{Cl}_2]\text{Cl}_2$ (Figure 7). $\text{Eu}_4\text{14}_4\text{Cl}_8$ is a tetranuclear complex with four eight-coordinate Eu^{II} centers, each connected to each other by bridging chloride ions. Of the four Eu^{II} centers, there are two different types of Eu^{II} ions. One is coordinated to three bridging chloride ions and one nonbridging chloride ion. *SHAPE* analysis of this Eu^{II} center showed the geometry to be biaugmented trigonal-prismatic. The second type of Eu^{II} center is coordinated to four bridging chloride ions and was found to

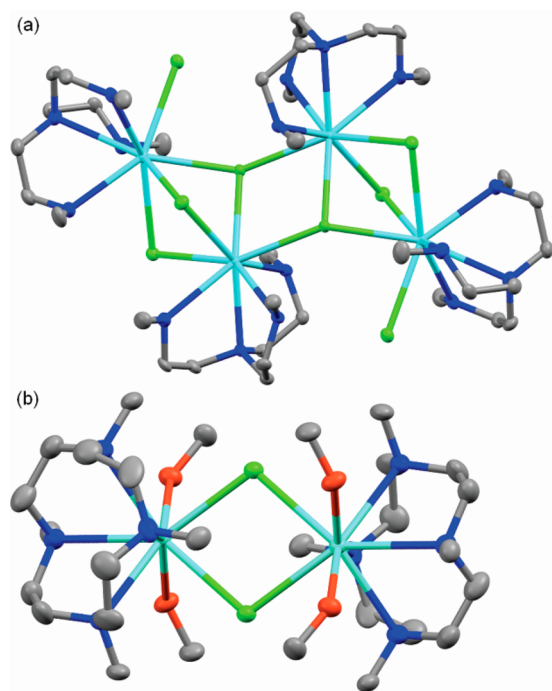


Figure 7. Molecular structures from the crystallographic data of (a) Eu_4Cl_8 and (b) $[\text{Eu}_{17}(\text{CH}_3\text{OH})_4\text{Cl}_2]\text{Cl}_2$. H atoms and non-coordinated counterions are omitted for clarity. Thermal ellipsoids are drawn at 50% probability. Color code: blue, N; gray, C; red, O; green, Cl; seagreen, Eu. The crystallographic data for each structure are available at the Cambridge Crystallographic Data Centre under the following deposition numbers: Eu_4Cl_8 , 2166710; $[\text{Eu}_{17}(\text{CH}_3\text{OH})_4\text{Cl}_2]\text{Cl}_2$, 2111610.

be a triangular dodecahedral geometry via *SHAPE* analysis. $[\text{Eu}_{17}(\text{CH}_3\text{OH})_4\text{Cl}_2]\text{Cl}_2$ is a dinuclear complex with two eight-coordinate Eu^{II} centers. The two Eu^{II} centers are connected to each other by two bridging chloride ions. Each Eu^{II} center is coordinated to two molecules of MeOH and four N atoms from **17**. *SHAPE* analysis of the Eu^{II} centers in $[\text{Eu}_{17}(\text{CH}_3\text{OH})_4\text{Cl}_2]\text{Cl}_2$ were calculated to be cubic geometry. The Eu–N bond lengths of Eu_4Cl_8 were between 2.69 and 2.88 Å, and the Eu–Cl bond lengths were between 2.92 and 3.13 Å. The Eu–N bond lengths for $[\text{Eu}_{17}(\text{CH}_3\text{OH})_4\text{Cl}_2]\text{Cl}_2$ were between 2.77 and 2.83 Å, the Eu–Cl bond lengths were 2.93 Å, and the Eu–O bond lengths were between 2.63 and 2.66 Å. The Eu–N and Eu–O bond lengths were within the range of previously reported lengths.^{22,28,29,34}

The complex $\text{Eu16}_2\text{Cl}_2$ was also evaluated by X-ray crystallography (Figure 8). X-ray-quality crystals were grown via slow evaporation from a concentrated solution of $\text{Eu16}_2\text{Cl}_2$ in MeOH. The resulting bright-orange crystals contained eight-coordinate Eu^{II} with two noncoordinating chloride counterions, similar to the recently reported structures of $[\text{Eu16}_2]\text{Br}_2$ and $[\text{Eu16}_2]\text{I}_2$.³⁵ Like these two structures, the crystal structure of $[\text{Eu16}_2]\text{Cl}_2$ is highly disordered. The Eu–N bond lengths in $[\text{Eu16}_2]\text{Cl}_2$ are between 2.65 and 2.72 Å, which is consistent with the Eu^{II} –N bond lengths from previously reported complexes of Eu16_2 .³⁵ To differentiate between the possibility of a square-prismatic or a square-antiprismatic structure, optimized geometries were calculated in both the gas phase and solution. These calculations were performed using the *Gaussian 16* suite of programs³⁶ using the

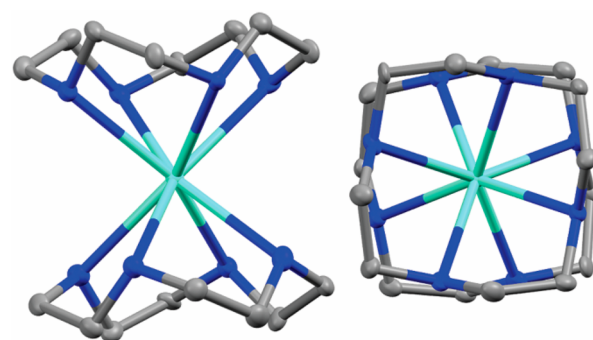


Figure 8. Molecular structures in crystals of $[\text{Eu}^{\text{II}}\text{16}_2]\text{Cl}_2$ (left) perpendicular to and (right) along the C_4 axis. H atoms and noncoordinated counterions are omitted for clarity. Thermal ellipsoids are drawn at 50% probability. Color code: blue, N; gray, C; seagreen, Eu. The crystallographic data for this structure are available at the Cambridge Crystallographic Data Centre under the deposition number 2059991.

UB3PW91 density functional with the Stuttgart–Dresden basis set for Eu.^{37–41} Optimization of Eu16_2 in MeOH with the SMD implicit solvation method⁴² yielded the square-antiprismatic structure. Attempts to optimize the square-prismatic structure led smoothly to the square-antiprismatic geometry, suggesting that the barrier for rotation is low, in accordance with the disorder seen in the crystal structure (Figure 8).

Identity of Complexes in Solution. Knowing the identity of $[\text{Eu16}_2]\text{Cl}_2$ and $[\text{Eu}_{17}(\text{CH}_3\text{OH})_4\text{Cl}_2]\text{Cl}_2$ in the solid state, we used Job plots to determine the stoichiometries of these complexes in solution (Figure 9).^{43,44} The absorbances for various mole ratios of **16** and **17** to EuCl_2 in MeOH were plotted. We attempted to make a Job plot for the complex between **13** and EuCl_2 ; however, the maximum absorbance peak for **13** was at 330 nm with a shoulder at 350 nm. The shoulder peak of $[\text{Eu13}_2]\text{Cl}_2$ at 350 nm only appears when there is ligand-to-metal ratio of greater than or equal to 10:1. This ligand-to-metal ratio is not within the bounds of a Job plot. Further, we were unable to construct Job plots based on absorbance for the other ligands because of the inability to differentiate between the absorbance of EuCl_2 in the presence and absence of the ligands. The mole ratio with the maximum absorbance for EuCl_2 and **16** was 0.5. This ratio is inconsistent with the 2:1 binding observed in the crystal structure $[\text{Eu16}_2]\text{Cl}_2$ (Figure 9a), and these results suggest a 1:1 ligand-to-metal ratio in solution between EuCl_2 and **16**. This difference in binding between EuCl_2 and **16** in solution and in the solid state is likely related to $[\text{Eu16}_2]\text{Cl}_2$ being partially soluble in MeOH. The complex that is 1:1 EuCl_2 -to-**16** is the complex that is soluble in MeOH and observed by UV–visible and luminescence spectroscopy, but the complex that is 1:2 EuCl_2 -to-**16** is the orange precipitate. With the optimized ground-state structures in solution (Figures S24–S27), time-dependent density functional theory was used to calculate the absorbance spectra of Eu13 , Eu13_2 , Eu16 , and Eu16_2 . The lowest-energy absorption bands are $f \rightarrow d$ transitions with spectra very similar to EuCl_2 . Calculated spectra with one ligand versus two ligands for **13** and **16** (Figures S28 and S29) support the Job plots of 1:1 complexes in solution. Calculated UV–visible spectra for two-ligand complexes have strong absorptions at long wavelength, contrary to that observed, whereas one-ligand complexes do not and agree better with the

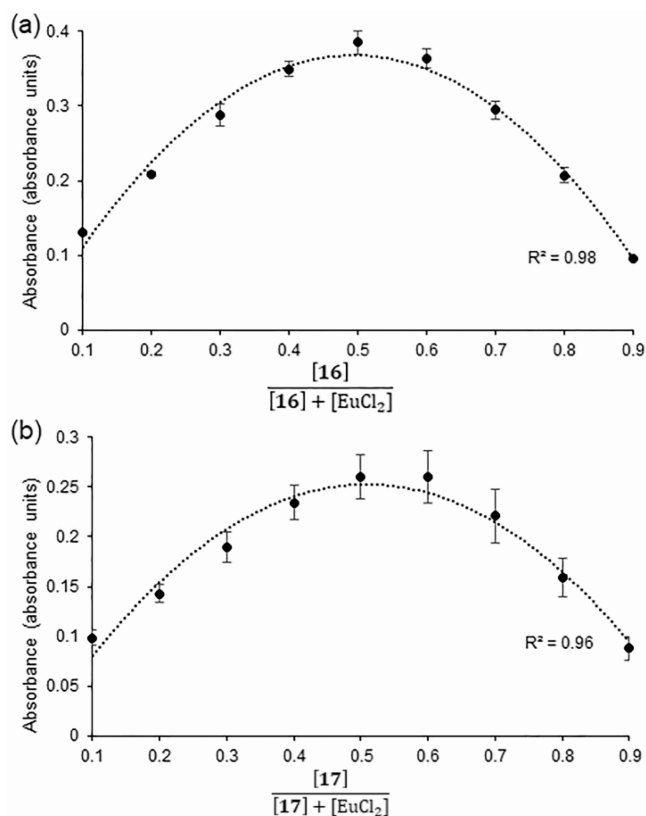


Figure 9. Job plots for EuCl_2 and (a) **16** and (b) **17** at wavelength 420 nm. The error bars represent the standard error of the mean of three independently prepared samples. The dotted lines denote a polynomial trend line.

observed spectra. The Job plot of EuCl_2 and **17** showed an outcome similar to that of the 1:1 ligand-to-metal ratio (Figure 9b). This 1:1 binding between EuCl_2 and **17** is consistent with the observed crystal structure of $[\text{Eu}_2\text{17}_2(\text{CH}_3\text{OH})_4\text{Cl}_2]\text{Cl}_2$.

Additional calculations were performed to explore the effect of explicit solvent molecules and counterions on the spectra for a 1:1 ligand-to-metal ratio. With a single ligand and implicit solvent, the peaks were at 370 nm for $\text{Eu}^{\text{II}}\text{13}$ and 380 nm for $\text{Eu}^{\text{II}}\text{16}$. When explicit solvent molecules and counterions were included in the calculations, they did not stay tightly coordinated to Eu. Specifically, for $\text{Eu}^{\text{II}}\text{13}$ with four explicit MeOH, one MeOH was 2.68 Å from Eu and the other three MeOH were 3.4–4.3 Å from Eu. The four MeOH remained hydrogen-bonded to each other. Similarly, for $\text{Eu}^{\text{II}}\text{16}$, one MeOH was 2.85 Å from Eu and the other MeOH were 3.2–3.3 Å from Eu, and all four MeOH were hydrogen-bonded to each other. For $\text{Eu}^{\text{II}}\text{13}$ and $\text{Eu}^{\text{II}}\text{16}$ with two MeOH and two Cl^- , only one MeOH and one Cl^- were coordinated to Eu. The other Cl^- was hydrogen-bonded to MeOH. The calculated spectra with explicit solvent molecules and counterions have peaks at 380 nm for $\text{Eu}^{\text{II}}\text{13}(\text{MeOH})_4$ and $\text{Eu}^{\text{II}}\text{16}(\text{MeOH})_4$, 390 nm for $\text{Eu}^{\text{II}}\text{13 Cl}_2(\text{MeOH})_2$, and 400 nm for $\text{Eu}^{\text{II}}\text{16 Cl}_2(\text{MeOH})_2$. These results indicate that the effect of the implicit solvent is comparable to adding a few explicit molecules along with the implicit solvent. A comparison with the observed spectra indicated that complexes with ligands **13** and **16** had only one ligand coordinated with Eu^{II} .

Electrochemical Studies. We evaluated the electrochemical potentials ($E_{1/2}$) of the $\text{Eu}^{\text{II/III}}$ couple in Eu_9Cl_2 , $[\text{Eu}\text{13}_2]\text{Cl}_2$, $[\text{Eu}\text{16}_2]\text{Cl}_2$, and $[\text{Eu}_2\text{17}_2(\text{CH}_3\text{OH})_4\text{Cl}_2]\text{Cl}_2$ be-

cause these complexes have absorptions that trail into visible light, making them potentially of interest as promoters of visible-light photoredox catalysis. The $E_{1/2}$ values of Eu_9Cl_2 , $[\text{Eu}\text{13}_2]\text{Cl}_2$, $[\text{Eu}\text{16}_2]\text{Cl}_2$, and $[\text{Eu}_2\text{17}_2(\text{CH}_3\text{OH})_4\text{Cl}_2]\text{Cl}_2$ were measured with cyclic voltammetry (Figure 10) to be 0.24, −0.62, −0.41, and −0.35 V versus NHE (Table 1). The excited-state potentials can be calculated via the Rehm–Weller formalism, which is $E_{1/2}^* - E_{0,0} = E_{1/2}^* - E_{1/2}$.

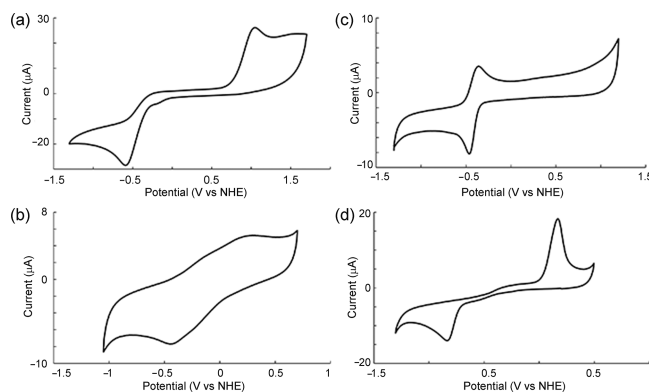


Figure 10. Cyclic voltammograms of (a) $\text{EuCl}_3 \cdot 6\text{H}_2\text{O}$ and **9** in water, (b) $\text{EuCl}_3 \cdot 6\text{H}_2\text{O}$ and **13** in water, (c) $\text{EuCl}_3 \cdot 6\text{H}_2\text{O}$ and **16** in water, and (d) $\text{EuCl}_3 \cdot \text{H}_2\text{O}$ and **17** in water.

Table 1. Maximum Absorptions and Emissions, $E_{1/2}$ Values, and $E_{1/2}^*$ Values of Mixtures of EuCl_2 and Ligands **1**, **9**, **13**, **16**, and **17**

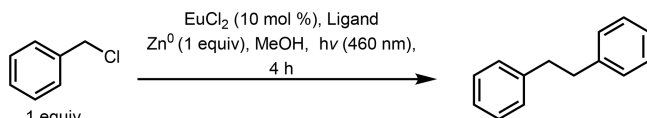
| ligand | absorbance (nm) | emission (nm) | $E_{1/2}^{\text{a}}$ | $E_{1/2}^{*\text{a}}$ |
|-----------|-----------------|---------------|----------------------|-----------------------|
| 1 | 460 | 580 | −0.70 | −2.8 |
| 9 | 340 | 480 | 0.24 | −2.3 |
| 13 | 330, 350 | 486 | −0.62 | −2.6 |
| 16 | 362 | 449 | −0.41 | −3.2 |
| 17 | 350 | 499 | −0.35 | −2.8 |

^aVolts versus NHE.

Using the ground-state $E_{1/2}$ values and emission, the calculated excited-state potentials ranged from −2.0 to −3.2 V versus NHE. The calculated excited-state potential of $\text{Eu}^{\text{II}}\text{1}$ is −2.8 V versus NHE. Because the calculated excited-state reduction potentials of $[\text{Eu}\text{13}_2]\text{Cl}_2$ and $[\text{Eu}\text{16}_2]\text{Cl}_2$ are close to the calculated excited-state reduction potential of $\text{Eu}^{\text{II}}\text{1}$ and they have absorptions into the visible-light region, we hypothesized that they might be viable promoters of visible-light-promoted photoredox catalysis.

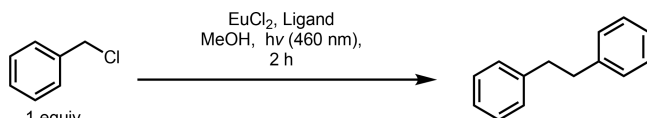
Reactivity. To evaluate the reactivity of $\text{Eu}^{\text{II}}\text{9}_3\text{Cl}_2$, $[\text{Eu}^{\text{II}}\text{13}_2]\text{Cl}_2$, $[\text{Eu}^{\text{II}}\text{16}_2]\text{Cl}_2$, and $[\text{Eu}_2\text{17}_2(\text{CH}_3\text{OH})_4\text{Cl}_2]\text{Cl}_2$ as photoredox catalysts, we performed benzyl chloride couplings with each complex (Table 2). Trials b–e in Table 2 were performed with **9**, **13**, **16**, and **17**, respectively, and with a 10:1 ligand-to- EuCl_2 ratio to push the equilibria toward complex formation. Thin-layer chromatography of trials b–e showed evidence of only benzyl chloride and no product formation. This lack of reactivity is likely because of the formation of Zn–ligand complexes in the reaction mixture due to the presence of Zn as the sacrificial reducing agent.^{46–49}

To study the reactivity outside the catalytic domain, we performed stoichiometric reactions by varying the ligand concentration with constant $[\text{EuCl}_2]$ for benzyl chloride coupling in the presence of blue light. We selected ligand/

Table 2. Benzyl Chloride Coupling Reactions


| trial | ligand | ligand/metal | yield (%) |
|-----------------|--------|--------------|------------|
| a ¹⁷ | 1 | 1:1 | 80 |
| b | 9 | 10:1 | no product |
| c | 13 | 10:1 | no product |
| d | 16 | 10:1 | no product |
| e | 17 | 10:1 | no product |

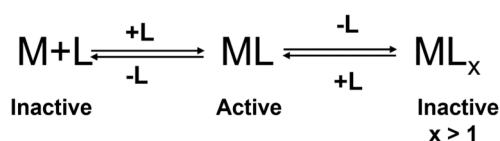
metal ratios of 1:1, 1.25:1, 2:1, 5:1, and 10:1 (Table 3). Yields for stoichiometric coupling reactions were determined via gas

Table 3. Yields (%) of Benzyl Chloride Coupling Reactions


| | ligand/metal | | | | |
|----|--------------|----------|----------|-----|----------|
| | 1:1 | 1.25:1 | 2:1 | 5:1 | 10:1 |
| 9 | 6 | 6 | 7 | 7 | 7 |
| 13 | 2 | 7 | 27 | 41 | 43 |
| 16 | 6 | 7 | 8 | 11 | 12 |
| 17 | <i>a</i> | <i>a</i> | <i>a</i> | <1 | <i>a</i> |

^aNo product.

chromatography–mass spectroscopy (GS–MS). We hypothesized that at lesser ligand-to-metal ratios, there would be a lack of formation of active complexes capable of promoting photochemical reactions, as evidenced by the poor reactivity observed in these reactions (Scheme 1, left). At greater ligand-

Scheme 1. Possible Reactivity of the Photochemical Promoter toward Benzyl Chloride

to-metal ratios, more than 1 equiv of ligand binds to the metal, inhibiting reactivity with the substrate, as evidenced by the formation of crystals of Eu^{II}16₂, that has a ligand-to-metal ratio different from that described in the Job plot (Scheme 1, right). From those reactions, the primary amine, 13, displayed the greatest reactivity compared to the secondary, 9 and 16, and tertiary, 17, amines. In the case of 13, small ligand-to-metal ratios resulted in poor yields. At moderate ligand-to-metal ratios, good reactivity was observed with no byproducts; however, at greater ligand-to-metal ratios, the yields were good, but the formation of byproducts of benzyl chloride addition to the ligand was observed. The aforementioned byproducts that were observed via GC–MS were found to be products of alkylation of the amine ligands. Alkylation was only observed with 9 and 13 in both light and dark conditions (Figures S18, S19, S22, and S23). Additionally, in the previous report,²² alkylation of azacryptand 1 was not observed, and therefore alkylation of 9 and 13 could be at least partially responsible for

the lower yields observed with 9 and 13 relative to 1. These observations are consistent with reactivity depending on the formation of metal–ligand complexes (ML) in the reaction mixture (Scheme 1). Furthermore, complexes that are closer to being electrochemically reversible (Figure 10) tend to produce greater yields. The formation of 1,2-diphenylethane promoted by [Eu13₂]Cl₂ shows that an open coordination site is likely required to promote reactivity. The activity of [Eu13₂]Cl₂ as a visible-light-promoted photoredox initiator indicates that a cryptand, such as ligand 1, which is the first reported Eu^{II}-containing photoredox catalyst,²² is not required to promote reactivity; however, the ability of 1 to evade interaction with Zn after complexation with Eu suggests that strong binding to Eu is essential for catalysis when Zn is used as the sacrificial reducing agent.

CONCLUSIONS

The studies reported have revealed an understanding of the ligand properties that provide favorable environments for visible-light-promoted photoredox catalysis using Eu^{II}. In general, the results suggest that ligands containing secondary amines promote a greater bathochromic shift in the absorbance of Eu^{II} than ligands containing primary or tertiary amines. Macrocyclic ligands tend to have a greater bathochromic shift on the absorbance of Eu^{II} than nonmacrocyclic ligands. A comparison of both macrocyclic and nonmacrocyclic ligands of varying denticity showed that ligands with larger denticities shift the absorbance of Eu^{II} more bathochromically than ligands with smaller denticities. The reactivity was explored with four ligands that displayed absorption spectra that trailed further into the visible-light region than EuCl₂. Of the ligands evaluated, complex Eu13₂Cl₂ was found to be the best promoter of the reductive coupling of benzyl chloride but revealed that, in the absence of strong binding to Eu, competition with Zn coordination or substitution of a ligand with a substrate is possible. These observations are promising for the development of future Eu^{II}-containing visible-light-promoted photoredox catalysts, and we are currently elucidating the scope of the reactivity of these complexes.

ASSOCIATED CONTENT

Supporting Information

The Supporting Information is available free of charge at <https://pubs.acs.org/doi/10.1021/acs.inorgchem.2c02911>.

Experimental procedures, absorbance and luminescence spectra, GC–MS data, SHAPE analysis, computational methods, and crystallographic data (PDF)

Accession Codes

CCDC 2059991, 2111610–2111612, 2121539, 2121631, 2166710, and 2209884 contain the supplementary crystallographic data for this paper. These data can be obtained free of charge via www.ccdc.cam.ac.uk/data_request/cif, or by emailing data_request@ccdc.cam.ac.uk, or by contacting The Cambridge Crystallographic Data Centre, 12 Union Road, Cambridge CB2 1EZ, UK; fax: +44 1223 336033.

AUTHOR INFORMATION

Corresponding Author

Matthew J. Allen – Department of Chemistry, Wayne State University, Detroit, Michigan 48202, United States;
 orcid.org/0000-0002-6868-8759; Email: mallen@chem.wayne.edu

Authors

Ramiro Barraza, Jr. – Department of Chemistry, Wayne State University, Detroit, Michigan 48202, United States

Alexander G. Sertage – Department of Chemistry, Wayne State University, Detroit, Michigan 48202, United States

Aravind B. Kajjam – Department of Chemistry, Wayne State University, Detroit, Michigan 48202, United States

Cassandra L. Ward – Lumigen Instrument Center, Wayne State University, Detroit, Michigan 48202, United States;

orcid.org/0000-0001-6736-6769

Jacob C. Lutter – Department of Chemistry and Biochemistry, University of Southern Indiana, Evansville, Indiana 47712, United States

H. Bernhard Schlegel – Department of Chemistry, Wayne State University, Detroit, Michigan 48202, United States;

orcid.org/0000-0001-7114-2821

Complete contact information is available at:

<https://pubs.acs.org/10.1021/acs.inorgchem.2c02911>

Author Contributions

The manuscript was written through contributions of all authors. All authors have given approval to the final version of the manuscript.

Notes

The authors declare no competing financial interest.

ACKNOWLEDGMENTS

This research was supported by the National Science Foundation (Grants CHE-1564755 and CHE-1856437), by NIH Grant T32 GM142519, and in part by NIGMS/NIH Grant R25 GM058905-20. X-ray crystallography was performed in the Lumigen Instrument Center, which is partially supported by NIH Grant 3R01 EB027103-02S1. We thank the Wayne State University computing grid for the computational time. We thank Prof. J. Stockdill for use of the GC–MS instrument.

REFERENCES

- (1) Tucker, J. W.; Stephenson, C. R. J. Shining Light on Photoredox Catalysis: Theory and Synthetic Applications. *J. Org. Chem.* **2012**, *77*, 1617–1622.
- (2) Candish, L.; Collins, K. D.; Cook, G. C.; Douglas, J. J.; Gómez-Suárez, A.; Jolit, A.; Keess, S. Photocatalysis in the Life Science Industry. *Chem. Rev.* **2022**, *122*, 2907–2980.
- (3) Wang, C.-S.; Dixneuf, P. H.; Soulé, J.-F. Photoredox Catalysis for Building C–C Bonds from C(sp²)–H Bonds. *Chem. Rev.* **2018**, *118*, 7532–7585.
- (4) Holmberg-Douglas, N.; Nicewicz, D. A. Photoredox-Catalyzed C–H Functionalization Reactions. *Chem. Rev.* **2022**, *122*, 1925–2016.
- (5) Romero, N. A.; Nicewicz, D. A. Organic Photoredox Catalysis. *Chem. Rev.* **2016**, *116*, 10075–10166.
- (6) Festa, A. A.; Voskressensky, L. G.; Van der Eycken, E. V. Visible Light-Mediated Chemistry of Indoles and Related Heterocycles. *Chem. Soc. Rev.* **2019**, *48*, 4401–4423.
- (7) Lammer, A. D.; Thiabaud, G.; Brewster, J. T., II; Alaniz, J.; Bender, J. A.; Sessler, J. L. Lanthanide Texaphyrins as Photocatalysts. *Inorg. Chem.* **2018**, *57*, 3458–3464.
- (8) Narayanam, J. M. R.; Stephenson, C. R. J. Visible Light Photoredox Catalysis: Applications in Organic Synthesis. *Chem. Soc. Rev.* **2011**, *40*, 102–113.
- (9) Chen, Y.; Mcnamara, N.; May, O.; Pillaiyar, T.; Blakemore, D. C.; Ley, S. V. Photoredox Generation of Sulfonyl Radicals and Coupling with Electron Deficient Olefins. *Org. Lett.* **2020**, *22*, 5746–5748.
- (10) Flodén, N. J.; Trowbridge, A.; Willcox, D.; Walton, S. M.; Kim, Y.; Gaunt, M. J. Streamlined Synthesis of C(sp³)-Rich N-Heterospirocycles Enabled by Visible-Light-Mediated Photocatalysis. *J. Am. Chem. Soc.* **2019**, *141*, 8426–8430.
- (11) Kim, T.; McCarver, S. J.; Lee, C.; MacMillan, D. W. C. Sulfonamidation of Aryl and Heteroaryl Halides through Photosensitized Nickel Catalysis. *Angew. Chem., Int. Ed.* **2018**, *57*, 3488–3492.
- (12) Zhao, W.; Wurz, R. P.; Peters, J. C.; Fu, G. C. Photoinduced, Copper-Catalyzed Decarboxylative C–N Coupling to Generate Protected Amines: An Alternative to the Curtius Rearrangement. *J. Am. Chem. Soc.* **2017**, *139*, 12153–12156.
- (13) Oderinde, M. S.; Jones, N. H.; Juneau, A.; Frenette, M.; Aquila, B.; Tentarelli, S.; Robbins, D. W.; Johannes, J. W. Highly Chemoselective Iridium Photoredox and Nickel Catalysis for the Cross-Coupling of Primary Aryl Amines with Aryl Halides. *Angew. Chemie - Int. Ed.* **2016**, *55*, 13219–13223.
- (14) Barraza, R., Jr.; Allen, M. Lanthanide Luminescence in Visible-Light-Promoted Photochemical Reactions. *Molecules* **2020**, *25*, 3892.
- (15) Prier, C. K.; Rankic, D. A.; MacMillan, D. W. C. Visible Light Photoredox Catalysis with Transition Metal Complexes: Applications in Organic Synthesis. *Chem. Rev.* **2013**, *113*, 5322–5363.
- (16) Shaw, M. H.; Twilton, J.; MacMillan, D. W. C. Photoredox Catalysis in Organic Chemistry. *J. Org. Chem.* **2016**, *81*, 6898–6926.
- (17) Larsen, C. B.; Wenger, O. S. Photoredox Catalysis with Metal Complexes Made from Earth-Abundant Elements. *Chem. Eur. J.* **2018**, *24*, 2039–2058.
- (18) Abderrazak, Y.; Bhattacharyya, A.; Reiser, O. Visible-Light-Induced Homolysis of Earth-Abundant Metal-Substrate Complexes: A Complementary Activation Strategy in Photoredox Catalysis. *Angew. Chem., Int. Ed.* **2021**, *60*, 21100–21115.
- (19) Fajardo, J., Jr.; Barth, A. T.; Morales, M.; Takase, M. K.; Winkler, J. R.; Gray, H. B. Photoredox Catalysis Mediated by Tungsten(0) Arylisocyanides. *J. Am. Chem. Soc.* **2021**, *143*, 19389–19398.
- (20) Bell, J. D.; Murphy, J. A. Recent Advances in Visible Light-Activated Radical Coupling Reactions Triggered by (i) Ruthenium, (ii) Iridium and (iii) Organic Photoredox Agents. *Chem. Soc. Rev.* **2021**, *50*, 9540–9685.
- (21) Rao, C. N.; Hoz, S. Photostimulated Reduction of Nitriles by SmI₂. *J. Org. Chem.* **2012**, *77*, 4029–4034.
- (22) Jenks, T. C.; Bailey, M. D.; Hovey, J. L.; Fernando, S.; Basnayake, G.; Cross, M. E.; Li, W.; Allen, M. J. First Use of a Divalent Lanthanide for Visible-Light-Promoted Photoredox Catalysis. *Chem. Sci.* **2018**, *9*, 1273–1278.
- (23) Enemærke, R. J.; Hertz, T.; Skrydstrup, T.; Daasbjerg, K. Evidence for Ionic Samarium(II) Species in THF/HMPA Solution and Investigation of Their Electron-Donating Properties. *Chem. Eur. J.* **2000**, *6*, 3747–3754.
- (24) Nimkar, A.; Maity, S.; Flowers, R. A., II; Hoz, S. Contrasting Effect of Additives on Photoinduced Reactions of SmI₂. *Chem. Eur. J.* **2019**, *25*, 10499–10504.
- (25) Corbin, B. A.; Hovey, J. L.; Thapa, B.; Schlegel, H. B.; Allen, M. J. Luminescence Differences between Two Complexes of Divalent Europium. *J. Organomet. Chem.* **2018**, *857*, 88–93.
- (26) Jenks, T. C.; Allen, M. J. Divalent Lanthanide Luminescence in Solution. In *Modern Applications of Lanthanide Luminescence*. De Bettencourt-Dias, A., Ed.; Springer: Cham, Switzerland, 2021; pp 67–92.
- (27) Jiang, J.; Higashiyama, N.; Machida, K.; Adachi, G. The Luminescent Properties of Divalent Europium Complexes of Crown Ethers and Cryptands. *Coord. Chem. Rev.* **1998**, *170*, 1–29.
- (28) Basal, L. A.; Kajjam, A. B.; Bailey, M. D.; Allen, M. J. Systematic Tuning of the Optical Properties of Discrete Complexes of Eu^{II} in Solution Using Counterions and Solvents. *Inorg. Chem.* **2020**, *59*, 9476–9480.
- (29) Yan, W.; Li, T.; Cai, Z.; Qi, H.; Guo, R.; Huo, P.; Liu, Z.; Bian, Z. Systematic Tuning of the Emission Colors and Redox Potential of

Eu(II)-Containing Cryptates by Changing the N/O Ratio of Cryptands. *Inorg. Chem. Front.* **2022**, *9*, 4794–4800.

(30) Coates, J.; Hadi, D.; Lincoln, S. The Preparation, Characterization and Solution Chemistry of Some Nickel(II) and Copper(II) Complexes of 1,4,7,10-Tetramethyl-1,4,7,10-Tetraazacyclododecane. *Aust. J. Chem.* **1982**, *35*, 903–909.

(31) Schmidt, H.; Lensink, C.; Xi, S. K.; Verkade, J. G. New Prophosphatranes: Novel Intermediates to Five-Coordinate Phosphatranes. *Z. Anorg. Allg. Chem.* **1989**, *578*, 75–80.

(32) Llunell, M.; Casanova, D.; Cirera, J.; Alemany, P.; Alvarez, S. *SHAPE*, version 2.1; Springer: Barcelona, Spain, 2013.

(33) Lundberg, D. An Overview of Eight- and Nine Coordinate N-donor Solvated Lanthanoid(III) and Actinoid(III) Ions. *J. Radioanal. Nucl. Chem.* **2018**, *316*, 849–854.

(34) Schädle, D.; Anwänder, R. Rare-Earth Metal and Actinide Organoimide Chemistry. *Chem. Soc. Rev.* **2019**, *48*, 5752–5805.

(35) Li, J.; Wang, L.; Zhao, Z.; Sun, B.; Zhan, G.; Liu, H.; Bian, Z.; Liu, Z. Highly Efficient and Air-Stable Eu(II)-Containing Azacryptates Ready for Organic Light-Emitting Diodes. *Nat. Commun.* **2020**, *11*, 5218.

(36) Frisch, M. J.; Trucks, G. W.; Schlegel, H. B.; Scuseria, G. E.; Robb, M. A.; Cheeseman, J. R.; Scalmani, G.; Barone, V.; Petersson, G. A.; Nakatsuji, H.; Li, X.; Caricato, M.; Marenich, A. V.; Bloino, J.; Janesko, B. G.; Gomperts, R.; Mennucci, B.; Hratchian, H. P.; Ortiz, J. V.; Izmaylov, A. F.; Sonnenberg, J. L.; Williams-Young, D.; Ding, F.; Lipparini, F.; Egidi, F.; Goings, J.; Peng, B.; Petrone, A.; Henderson, T.; Ranasinghe, D.; Zakrzewski, V. G.; Gao, J.; Rega, N.; Zheng, G.; Liang, W.; Hada, M.; Ehara, M.; Toyota, K.; Fukuda, R.; Hasegawa, J.; Ishida, M.; Nakajima, T.; Honda, Y.; Kitao, O.; Nakai, H.; Vreven, T.; Throssell, K.; Montgomery, J. A., Jr.; Peralta, J. E.; Ogliaro, F.; Bearpark, M. J.; Heyd, J. J.; Brothers, E. N.; Kudin, K. N.; Staroverov, V. N.; Keith, T. A.; Kobayashi, R.; Normand, J.; Raghavachari, K.; Rendell, A. P.; Burant, J. C.; Iyengar, S. S.; Tomasi, J.; Cossi, M.; Millam, J. M.; Klene, M.; Adamo, C.; Cammi, R.; Ochterski, J. W.; Martin, R. L.; Morokuma, K.; Farkas, O.; Foresman, J. B.; Fox, D. J. *Gaussian 16*, revision B.01; Gaussian, Inc.: Wallingford, CT, 2016.

(37) Becke, A. D. Density-functional Thermochemistry. III. The Role of Exact Exchange. *J. Chem. Phys.* **1993**, *98*, 5648–5652.

(38) Perdew, J. P. Density-Functional Approximation for the Correlation Energy of the Inhomogeneous Electron Gas. *Phys. Rev. B* **1986**, *33*, 8822–8824.

(39) Perdew, J. P.; Burke, K.; Wang, Y. Generalized Gradient Approximation for the Exchange-Correlation Hole of a Many-Electron System. *Phys. Rev. B* **1996**, *54*, 16533–16539.

(40) Cao, X.; Dolg, M. Valence Basis Sets for Relativistic Energy-Consistent Small-Core Lanthanide Pseudopotentials. *J. Chem. Phys.* **2001**, *115*, 7348–7355.

(41) Cao, X.; Dolg, M. Segmented Contraction Scheme for Small-Core Actinide Pseudopotential Basis Sets. *J. Mol. Struct.* **2004**, *673*, 203–209.

(42) Marenich, A. V.; Cramer, C. J.; Truhlar, D. G. Universal Solvation Model Based on Solute Electron Density and on a Continuum Model of the Solvent Defined by the Bulk Dielectric Constant and Atomic Surface Tensions. *J. Phys. Chem. B* **2009**, *113*, 6378–6396.

(43) MacCarthy, P. Simplified Experimental Route for Obtaining Job's Curves. *Anal. Chem.* **1978**, *50*, 2165–2165.

(44) Renny, J. S.; Tomasevich, L. L.; Tallmadge, E. H.; Collum, D. B. Method of Continuous Variations: Applications of Job Plots to the Study of Molecular Associations in Organometallic Chemistry. *Angew. Chem., Int. Ed.* **2013**, *52*, 11998–12013.

(45) Rehm, D.; Weller, A. Kinetics of Fluorescence Quenching by Electron and H-Atom Transfer. *Isr. J. Chem.* **1970**, *8*, 259–271.

(46) Interrante, L. Complexes of Zinc (II) with Tris (2-Aminoethyl) Amine. *Inorg. Chem.* **1968**, *7*, 943–949.

(47) Canary, J. W.; Xu, J.; Castagnetto, J. M.; Rentzperis, D.; Marky, L. A. Enthalpic Control of Zinc-Water Acidity in Complexes of Tris(2-Aminoethyl)Amine and Tris(2-(Dimethylamino)Ethyl)-Amine. *J. Am. Chem. Soc.* **1995**, *117*, 11545–11547.

(48) Shionoya, M.; Kimura, E.; Shiro, M. A New Ternary Zinc(II) Complex with [12]AneN₄ (=1,4,7,10-Tetraazacyclododecane) and AZT (=3'-Azido-3'-Deoxythymidine). Highly Selective Recognition of Thymidine and Its Related Nucleosides by a Zinc(II) Macrocyclic Tetraamine Complex with Novel Complement. *J. Am. Chem. Soc.* **1993**, *115*, 6730–6737.

(49) Yang, R.; Zompa, L. J. Metal Complexes of Cyclic Triamines. I. Complexes of 1,4,7-Triazacyclononane ([9]AneN₃) with Nickel(II), Copper(II), and Zinc(II). *Inorg. Chem.* **1976**, *15*, 1499–1502.

Recommended by ACS

High-Entropy Layered Rare Earth Hydroxides

M.A. Teplonogova, V.K. Ivanov, *et al.*

NOVEMBER 23, 2022
INORGANIC CHEMISTRY

READ 

Anion-Manipulated Hydrolysis Process Assembles of Giant High-Nucleation Lanthanide-Oxo Cluster

Hai-Ling Wang, Hua-Hong Zou, *et al.*

NOVEMBER 29, 2022
INORGANIC CHEMISTRY

READ 

Dynamics of the Energy Transfer Process in Eu(III) Complexes Containing Polydentate Ligands Based on Pyridine, Quinoline, and Isoquinoline as Chromophoric A...

Albano N. Carneiro Neto, Fabio Piccinelli, *et al.*

OCTOBER 06, 2022
INORGANIC CHEMISTRY

READ 

Role of the Meso Substituent in Defining the Reduction of Uranyl Dipyrrin Complexes

Karlotta van Rees, Jason B. Love, *et al.*

DECEMBER 06, 2022
INORGANIC CHEMISTRY

READ 

Get More Suggestions >